Sensors & Actuators: B. Chemical 436 (2025) 137727

Contents lists available at ScienceDirect

Sensors and Actuators: B. Chemical

journal homepage: www.elsevier.com/locate/snb

Analyzing the cross-sensitivities of a zeolite-based ammonia sensor for SCR systems for application in the flue gas of biogenic waste combustion

Thomas Wöhrl *, Ralf Moos, Gunter Hagen

Department of Functional Materials, Center of Energy Technology (ZET), University of Bayreuth, Bayreuth 95447, Germany

ARTICLE INFO

Keywords:
Biomass combustion
Flue gas aftertreatment
Selective catalytic reduction
Ammonia detection
Zeolite-based capacitive gas sensor
Cross-sensitivities

ABSTRACT

In many applications for exhaust gas aftertreatment, ammonia is added to the flue gas as a reducing agent for nitrogen oxide (NO_x) emissions. An effective dosing control is necessary to avoid low NO_x conversion or ammonia slip. The here-investigated capacitive zeolite-based sensor helps to monitor the concentration of ammonia in the flue gas. For the specific application of biomass combustion plants, preliminary sensor investigations have been carried out in the laboratory. Special emphasis was given on investigating cross-sensitivities that could be caused by the large number of other components in the flue gas. An impressing selectivity was found. By adjusting the composition of the zeolite functional film and the operating temperature, the remaining small influences of NO_x and water vapor could be even further reduced. The described sensor concept should be an ideal solution for improving the NO_x aftertreatment efficiency.

1. Introduction

The interest in the use of biomass as an alternative to fossil energy sources has increased in recent years, mainly since fossil fuels contribute predominantly to climate change [1]. As a part of renewable energy, biomass offers a significant advantage in providing an energy supply that is independent of location and weather conditions [2]. Nevertheless, the use of wood-based biomass as an energy source to generate electricity or heat is discussed controversially [3]. CO_2 that is bound in wood is released back into the environment through combustion [4]. However, when used as a building material, it would be bound in the long term and, therefore, mathematically enable negative CO_2 emissions [5].

For this reason, there are numerous proposals to utilize biogenic waste materials for energy production that are by-products of agriculture and forestry not to be used for other purposes [6]. This improves the CO_2 balance by making more efficient use of available resources [7]. Biogenic waste includes materials such as bark, straw, or leaves, which are preferably processed into pellets before burning.

On the other hand, the combustion of biogenic residues and waste generates large quantities of substances, some of which are harmful to health [8], including sulfur or chlorine compounds, but also hydrocarbons or nitrogen oxides [9]. During the growth of biomass, various substances present in the soil are bound in such fuels and are subsequently released during combustion [10]. For this reason, aftertreatment of flue gases is an important requirement for power plants in order to maintain environmental compatibility [11].

Systems for the combustion of such substances are generally used to provide a local heating network and typically have thermal or electrical outputs in the range of more than 100 kW [12]. New legislation sets new limits for nitrogen oxide emissions [13]. Primary exhaust aftertreatment measures alone, such as combustion air control, are not anymore sufficient to meet with these limits [14]. Therefore, SCR (Selective Catalytic Reduction) systems will have to be installed to an increasing extent in the future. Here, ammonia (NH_3) is added to the flue gas, serving as a reducing agent for nitrogen oxides in the exhaust [15]. NH_3 is usually injected in the form of a liquid urea-water solution (AdBlue™) that evaporates due to the high exhaust temperatures and then decomposes into ammonia [16]. On an SCR catalyst (usually consisting of zeolites or mixed metal oxides such as VWT), the nitrogen oxides react with adsorbed ammonia to form molecular oxygen and nitrogen according to the following two equations [17,18]:

$$\text{Standard SCR: } 4\,NH_3 + 4\,NO + O_2 \rightarrow 4\,N_2 + 6\,H_2O \quad (1)$$

$$\text{Fast SCR: } 4\,NH_3 + 2\,NO + 2\,NO_2 \rightarrow 4\,N_2 + 6\,H_2O \quad (2)$$

This technology is well established in power plants and automotive applications. In the standard SCR reaction according to equation (1),

* Corresponding author.
E-mail address: functional.materials@uni-bayreuth.de (T. Wöhrl).

https://doi.org/10.1016/j.snb.2025.137727
Received 21 November 2024; Received in revised form 11 March 2025; Accepted 28 March 2025
Available online 31 March 2025
0925-4005/© 2025 The Authors. Published by Elsevier B.V. This is an open access article under the CC BY license (http://creativecommons.org/licenses/by/4.0/).

only nitrogen monoxide (NO) is reduced, whereas in equation (2) a faster reaction takes place with an equal amount of NO and NO_2. As a result, higher NO_x conversions can be achieved.

Due to the increasing demands for enhanced efficiency in SCR systems, further developments have been given in the field of SCR catalyst materials in recent years. Emphasis has been given on improving the long-term stability and NO_x conversion of catalysts over a wider temperature range. Investigations into SCR catalysts containing Mn or Ce have shown promising results due to increased specific surface and redox ability at low temperature (< 200 °C), although the formation of undesired by-products, such as N_2O, remains a challenge [19–21].

Recent advancements in flue gas aftertreatment technology, not only for biomass combustion, include the development of SCR catalysts in combination with particle filters. These catalysts are designed using suitable material combinations to reduce NO_x emissions while filtering particulate matter [22]. In order to prevent a rapid deactivation or poisoning of the catalytic converters, upstream dust collectors (e.g., cyclones or electrostatic precipitators) are used to remove a major proportion of the particles before they reach the SCR filter [23,24]. Especially for systems in the 100 kW range, acquisition and operating costs play a major role for cost-effectiveness.

Efficient operation of the exhaust aftertreatment system requires precise control of the AdBlue dosage to avoid too low NO_x conversion due to underdosing or NH_3 slip due to overdosing. The development of adapted nozzles for AdBlue™ dosing has been shown to result in the formation of finer droplets in the exhaust pipe, thereby enhancing the decomposition to ammonia [25]. The integration of additional mixing units has been found to lead to a more homogeneous mixing of gas components and an optimized use of the catalytic converter area [26].

Nevertheless, monitoring of emissions is often necessary, and is in certain cases, required by law. In gas- or coal-fired power plants, complex measurement systems such as FTIR, NDIR spectrometers or other optical principles with high accuracy are used for this purpose [27]. However, due to the high initial costs of such instruments, smaller combustion plants in the 100 kW to 1 MW range cannot be operated profitably. As a result, a large proportion of the operating costs would be spent on exhaust gas aftertreatment alone [23].

In the automotive sector, AdBlue™ dosing control is based on the measured values of several NO_x sensors up- and downstream of the SCR catalytic converter. In addition, the systems are based on complex characteristic curves determined on test benches. Due to the existing cross sensitivity of the used dual chamber NO_x sensors to ammonia, a sum signal of NO_x and NH_3 is measured [28]. Based on various engine parameters, such as exhaust gas temperature and load range, the characteristic curves can be used to control the AdBlue dosage [29]. However, these systems are now reaching their limits due to the continuously lower emission limits. Since systems for the combustion of biogenic residues and waste materials are usually custom-made and produced in small quantities, the effort to determine characteristic curves is not possible or at least not economically efficient [11].

For all these reasons, there is interest in selective ammonia sensors that meet the high demands of the harsh environment of biomass combustion flue gas. A wide range of ammonia sensors is available on the market for different applications. The most widely used principles include resistive gas sensors [30]. The use of semiconducting metal oxides or conducting polymers results in a large number of different versions [31]. While high availability ensures low acquisition costs for such sensors, long-term stability remains a significant challenge, particularly when deployed in harsh environments such as the biomass combustion flue gas. Optical gas sensors, based on the principle of absorbing light at a gas-specific wavelength, offer a good long-term stability because of their missing chemical interaction between gas and sensor [32,33]. Nevertheless, due to the relatively high system costs, coupled with the still often large dimensions of these sensor setups, further development work is necessary to produce a market-ready solution [34]. Furthermore, advancements have been made in the domain of field-effect transistor-based gas sensors (FET). Here, gas-sensitive materials are used at the gate or in the channel that influence the threshold voltage or drain current depending on the corresponding gases [35]. The implementation of SiC-FET-based gas sensors has already been demonstrated to effectively regulate an SCR exhaust gas aftertreatment system in a series of successful tests [36]. Mixed potential sensors also represent one of the most extensively researched sensor types for the detection of ammonia in exhaust gases [37–39]. Here, a potential difference is produced as a consequence of differing electrochemical reactions occurring at two electrodes [40]. This can be attributed to either a local separation of the electrodes or the coating of an electrode with an active layer, which results in divergent atmospheres at the two electrodes [41]. V_2O_5-WO_3-TiO_2 (VWT) is a commonly applied coating material that is also used as an SCR catalyst due to its ammonia adsorption properties [42]. Furthermore, it has been shown that the resistance of a VWT coating decreases when ammonia is adsorbed on the VWT coating [43,44].

This study presents a further type of an impedance-based ammonia sensor for use at high temperatures. The functional principle of the sensor is based on the changing permittivity of a zeolite layer when sorbing ammonia molecules. Zeolites are widely used in technical applications due to their adsorption properties and catalytic activity. In the field of exhaust gas aftertreatment, the application of zeolites is expanding as a result of the increasing demands on the efficiency of emission reduction. During the initial start-up phase of combustion engines, zeolite-based catalysts temporarily adsorb HC and CO molecules until the light-off temperature of the oxidation catalyst is reached [45]. However, zeolites are mostly used as SCR catalytic converters to reduce nitrogen oxide emissions. The long-term stability and high selectivity of zeolites turn it into a suitable material for a functional film in gas sensors. The sensor properties depend on the composition and structure of the zeolites. For instance, sensors that are sensitive to H_2, CO, or NO_x can be achieved by modified zeolites with Sn or Si, thereby combining the high sensitivity of semiconductor metal oxide sensors with the high selectivity of zeolite-based sensors [46,47].

Standard zeolites utilized in SCR catalysts materials are appropriate for ammonia sensitive film of a gas sensor [48,49]. Due to the presence of numerous gas components in the flue gas, potential cross-sensitivities are a special challenge and of particular importance for the planned future application in biomass combustion systems. The focus is on gases that are expected to be present in high concentrations, such as H_2O, NO_x, O_2, or CO.

2. Experimental

The requirements for the sensor are low production and operation costs, high selectivity, and high temperature stability. This section discusses in more detail how this was achieved.

2.1. Sensor design and functionality

The sensor is manufactured in planar thick-film technology, a cost-effective production technology that has already been described in detail in [50]. The rear side is equipped with a platinum heater structure, which enables the sensor to reach temperatures exceeding 300 °C during operation. The front surface features an interdigital electrode (IDE) structure with a line width and spacing of 20 µm. The capacitance of the IDE structure at room temperature without functional layer is approximately 43 pF. The manufacturing of one sensor element requires only small quantities of gold (DuPont 5744 R; ~65 mg) and platinum paste (Heraeus LPA88–11S; ~90 mg). Furthermore, glass-containing insulation layers protect the heater and the leads to the IDE structure and, furthermore, ammonia is prevented from being oxidized by the catalytically active platinum heater structure. In addition, the insulation layer reduces the risk of short circuits between the feed lines due to the accumulation of conductive soot particles on the sensor surface. Fig. 1

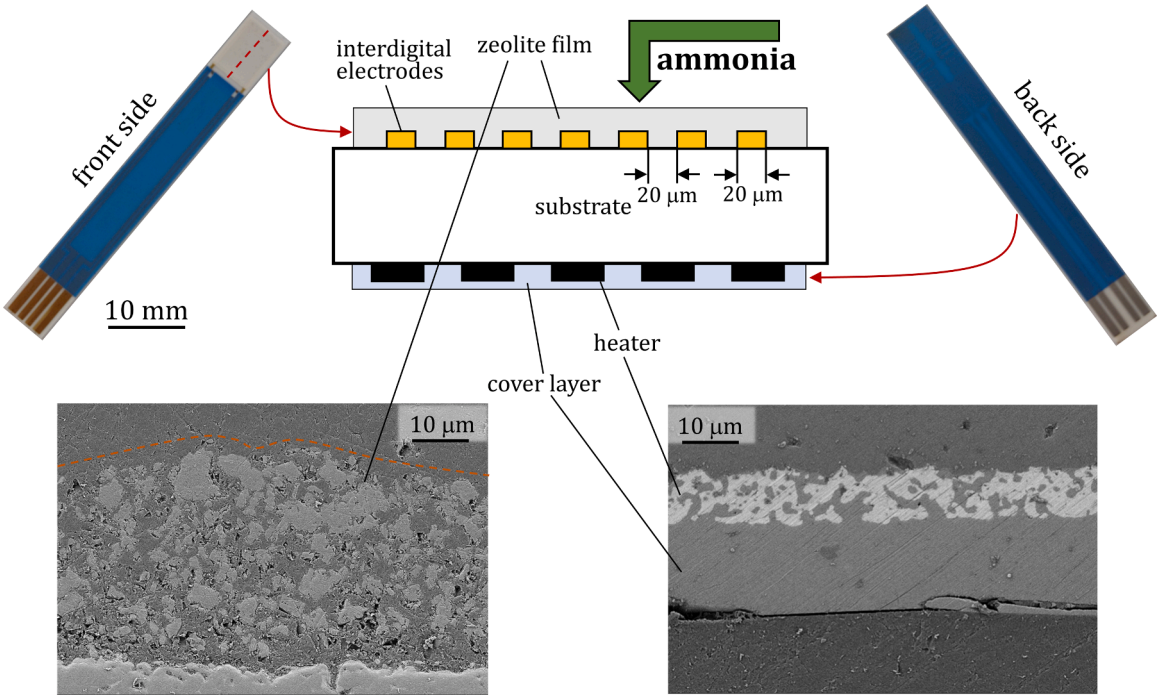

Fig. 1. Structure of the sensor element based on a schematic drawing and SEM images of the cross-section with screen-printed zeolite film, heater structure, and cover layer on an alumina substrate.

provides a schematic cross-section of the sensor element. The SEM images also illustrate the high porosity of the zeolite film.

In order to detect ammonia, a gas sensitive zeolite film is applied on top of the IDE structure. The zeolite film exhibits a specific electrical behavior that is directly correlated with the concentration of ammonia present in the gas [51]. These properties depend on the selected zeolite [52].

2.2. Zeolite structure and composition

Zeolites consist of AlO_4^- and SiO_4 tetrahedra (primary components) that form microporous cavity structures [53]. The primary components are linked via oxide corners, which in turn form secondary and then ternary structures [54]. This allows the formation of a diverse range of structural configurations. For ZSM-5 zeolites used in this study, a 10-ring structure with a pore size of approximately 0.5–0.6 nm [55,56] is formed. The porous structure of zeolites enables molecular diffusion to the inner surface of the zeolite [57].

A parameter of specific interest in the technical application of zeolites, particularly in relation to their adsorption properties, is the module [58]. This value defines the SiO_2/Al_2O_3 molar ratio within the zeolite structure. The different oxidation states of silicon (+IV) and aluminum (+III) yield in a negative charge within the zeolite cage that must be balanced by a proton or another cation. In the case of the H-ZSM-5 zeolite used here, this charge equalization occurs with a proton (H^+-ion) [59]. Additionally, the module is correlated with the number of active centers at which the gas species can adsorb [60]. A lower module indicates a higher proportion of aluminum atoms and, consequently, a higher number of active centers in the zeolite [61].

However, it is important to distinguish between different acid centers and binding types. As previously described in literature, the Brønsted centers, Lewis centers, and terminal silanol groups show varying binding strengths and acidities [62]. The characterization of these bonds is typically determined by TPD (temperature-programmed desorption) measurements using ammonia as desorbing molecule. At the beginning, the zeolite is fully loaded with ammonia at temperatures below 100 °C. Subsequently, the zeolite is continuously heated, resulting in a temperature-dependent desorption of ammonia [63]. The detected peaks can then be attributed to the corresponding bonding types.

This sorption processes serve as the fundamental operating principle of the sensor. The temperature of the sensor is selected in order to achieve an equilibrium between the adsorption and desorption of ammonia. As a consequence of a change in the electrical properties of the zeolite as a response of the amount of ammonia that has been adsorbed, it is possible to measure a concentration-dependent signal [64]. The sensitivity of the sensor to ammonia depends on several factors, including the specific zeolite utilized. The following measurements refer to ZSM-5 zeolites in the H-form, which have a module of 27, 55, or 300 (supplier: ALSI-Penta Zeolite GmbH; zeolite SH-27, 55, 300). These materials have a specific surface area of $S_{BET,m27} = 313\ m^2/g$, $S_{BET,m55} = 302\ m^2/g$ and $S_{BET,m300} = 368\ m^2/g$, as determined with nitrogen using the BET method.

The zeolites in powder form were processed to a paste that is suitable for screen-printing using a viscous medium (ethylcellulose-terpineol in a weight ratio of approximately 1:1 to the zeolite powder). For this, the powder was initially mixed manually with the fluid before being processed in a three-roll mill (Exakt 50 Ointment Mill). This process was repeated until a homogeneous, viscous mass was obtained that is suitable for being used as a screen-printing paste. Subsequently, the paste was printed onto the sensors, followed by a drying step at 120°C for 15 minutes. Finally, the zeolite films were fired at 850 °C. The heating and cooling rates during the firing process were set to around 30 K/min and the dwell time at the maximum temperature was 20 min. The firing process of the paste leads to the removal of the organic components, which results in a high porosity of the zeolite layer (see Fig. 1). In addition, the high firing temperature improved the adhesion of the layer to the carrier substrate, but also slightly reduced the specific surface compared to lower firing temperatures [56]. Attempts with diluted pastes, i.e., with a lower proportion of the zeolite powder, resulted in an inhomogeneous layer thickness with significantly reduced reproducibility and adhesion of the layer.

The zeolite layer thickness (in the fired state) was approximately 35 micrometers. It was determined by a laser scanning microscope (Zeiss LSM900) and is an average value of several measurement points along

the zeolite surface. The layer thickness was also confirmed by the SEM image in Fig. 1.

2.3. Measurement setup

The sensors were evaluated in a test bench for synthetic flue gas. The concentrations of the components in the gas were selected to represent the typical range of values observed in the flue gas of biomass combustion processes. The base gas was composed primarily of CO_2 (3 vol %), O_2 (10 vol%), and gaseous H_2O (5 vol%) in N_2. The concentrations of the base gas components were selected on the basis of values from real biomass combustion, which can, however, vary depending on the type of fuel and on the operation mode of the boiler [9]. Considering the water content, concentrations in the range of 10 % can also be achieved and will be addressed below [13]. The total flow rate through a cylindrical measuring chamber with an internal diameter of 40 mm was 6 L/min. To determine the ammonia response of the sensor, the ammonia concentration was varied between 0 and 240 ppm at a constant flow rate. In order to obtain concentrations in the desired range, a pre-diluted gas cylinder with 9.9 vol% NH_3 in N_2 was used. This concentration range for ammonia is based on literature data on the NO_x emissions of different biogenic fuels. For the most common fuels, such as straw, miscanthus, or rice husks, a concentration range of up to approximately 300 ppm is obtained [9]. According to equations (1) and (2), the NH_3/NO_x ratio should be around 1:1 for optimum NO_x conversion. To prevent NH_3 slip, NH_3 is often underdosed to a certain extent [29]. In consequence, the selected concentration range for ammonia is slightly lower. To minimize the potential for adsorption and desorption processes of ammonia on the steel piping of the system, the supply lines to the measuring chamber were heated to approximately 120 °C, and the measuring chamber itself was heated to approximately 70 °C [65]. Nevertheless, a slight delay in the response to changes in ammonia concentration can still be observed by the downstream FTIR spectrometer (MKS MultiGas 2030 FTIR Analyzer). Concurrently, the FTIR was used to verify the actual ammonia dosage and for comparison with the sensor data.

The sensor values were logged using a measuring device for electrochemical impedance analysis (PalmSens 4). Initially, impedance spectra were recorded in the frequency range between 1 MHz and 0.1 Hz with the aim of evaluating the frequency-dependent electrical behavior of the sensors. Subsequently, measurements were conducted at a constant excitation frequency ($f = 700$ kHz) to determine the capacitance of the sensor with enhanced temporal resolution. In both cases, the effective excitation voltage was set to $U_{eff} = 250$ mV.

Digital electronics were used to control the temperature of the sensor by measuring the four-wire resistance of the platinum heater structure on the reverse side of the sensor. The operating temperature of the sensor could be set independently of the flow conditions in the measuring chamber by means of a previously determined characteristic curve (which shows only slight deviations from the standardized characteristic curve of a platinum temperature sensor). The heaters were calibrated by measuring the resistance at room temperature [66].

3. Results and discussion

The following measurements primarily focused on the sensor behavior of various zeolite modules in regard to ammonia, as well as their cross-sensitivities when dosing different gas components.

3.1. Effect of module variation on ammonia sensitivity

Zeolites with three different modules were initially compared by recording impedance spectra within the frequency range between 1 MHz and 0.1 Hz. The sensors were heated to a temperature of 400 °C. Following an initial measurement at base gas without ammonia, the concentration was then increased to 48 and 240 ppm. The results are shown in Fig. 2.

The measurements indicate that, regardless of the module of the zeolite layer, the sensors behave similarly. Their impedance spectra can be described by a parallel *RC* element with blocking electrodes (visible at low frequencies) [67,68]. The low electrical conductivity of zeolites results in impedances in the order of several megohms for low frequencies. It originates predominantly from the transport of protons, which are present as charge balancing ions [69]. The (ionic) conductivity is thus influenced by the module of the zeolite, which affects the proton transport path [69]. Therefore, the proton conductivity of a zeolite with a low module and a high number of active centers is higher due to its shorter path length. Consequently, the diameters of the respective semicircles illustrated in the Nyquist plot decrease for zeolites with lower modules.

The adsorption of molecules (in this case, ammonia) on the zeolite affects the proton transport. Literature describes several temperature-dependent conductivity mechanisms [70–72]. It has been demonstrated that an enhanced transport of protons along the solvate molecules is occurring. This results in a reduction of the radius of the

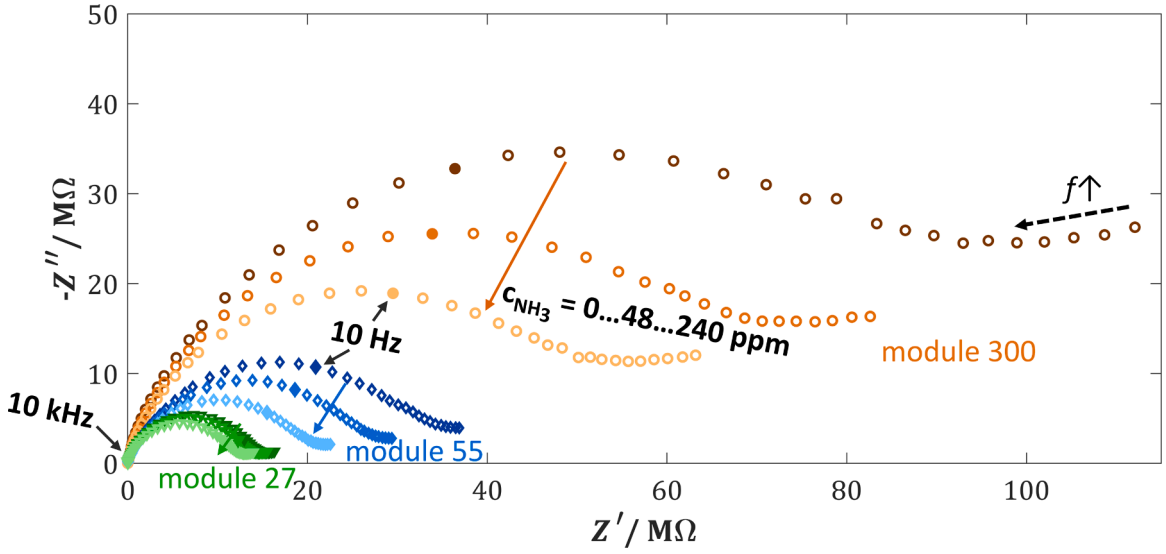

Fig. 2. Impedance spectra (1 MHz - 0.1 Hz) of H-ZSM-5 zeolite sensors with different modules (27, 55, 300) under variation of the ammonia concentration (0, 48, 240 ppm); sensor temperature 400 °C, base gas composition: 10 vol% O_2, 3 vol% CO_2, 5 vol% H_2O in N_2.

semicircle observed in the Nyquist plot impedance spectrum. This effect can be seen in Fig. 2 for sensors of each the examined zeolite modules.

In order to obtain measurements with a higher timely resolution, data acquisition was carried out at a constant excitation frequency. For the sensors examined here, the phase angle φ remained within the range of −75° to −85° at frequencies higher than 10 kHz. This is almost analogous to the behavior characteristic of a capacitor, whereby changes in permittivity result in corresponding alterations in capacitance [73]. There have also been studies in literature on the influence of adsorption processes on the permittivity of zeolites in a wide frequency range (mHz – GHz) [74,75]. Changes in the permittivity of the zeolite structure are due to dipole moment variations, which are attributed to the movement of protons and modifications in bond distances of the lattice [76,77]. Consequently, the sensor capacitance C is calculated using the data obtained from the impedance analysis. In addition to the phase angle φ and the excitation frequency f, the absolute value of the impedance $|Z|$ is of particular importance for the calculation of the capacitance (see equation (3)):

$$C = \frac{\sin(-\varphi)}{2\pi \bullet f \bullet |Z|} \tag{3}$$

A capacitive measurement conducted at an excitation frequency of 700 kHz leads to impedance values in the range of kiloohms. Consequently, inaccuracies resulting from the measurement of low currents can be avoided. Moreover, future evaluations can be carried out with the measurement units of MEMS components. Such sensors, like acceleration sensors or gyroscopes, are often based on a capacitive principle [78–80].

Fig. 3a illustrates the time course of continuous capacitance measurements of sensors with different zeolite films (module 27, 55, 300). The concentration of ammonia was increased stepwise between 0 and 240 ppm (see Fig. 3b), and the time-dependent capacitance values of the sensors were determined simultaneously.

The base capacitance of all sensors, defined as the capacitance value measured before test gas admixture (0–7 min) were in a similar range between 53 and 61 pF. The differences between the sensors cannot only be attributed to influences resulting from the positioning of the cables, variations in layer thickness, or the presence of minor defects in the IDE structure, but also to the composition of the zeolite layer. As expected, zeolites with a higher number of protons (lower module) contribute more significantly to permittivity and, consequently, to the sensor capacitance [81].

The response of the sensors varied depending on the specific zeolite module. To study in detail, the change in capacitance (in relation to the base capacitance in the base gas) as a function of the ammonia concentration was evaluated and is illustrated in Fig. 3c.

In general, characteristic curves of the sensors are similar to adsorption isotherms (Freundlich isotherm) [82]. However, notable

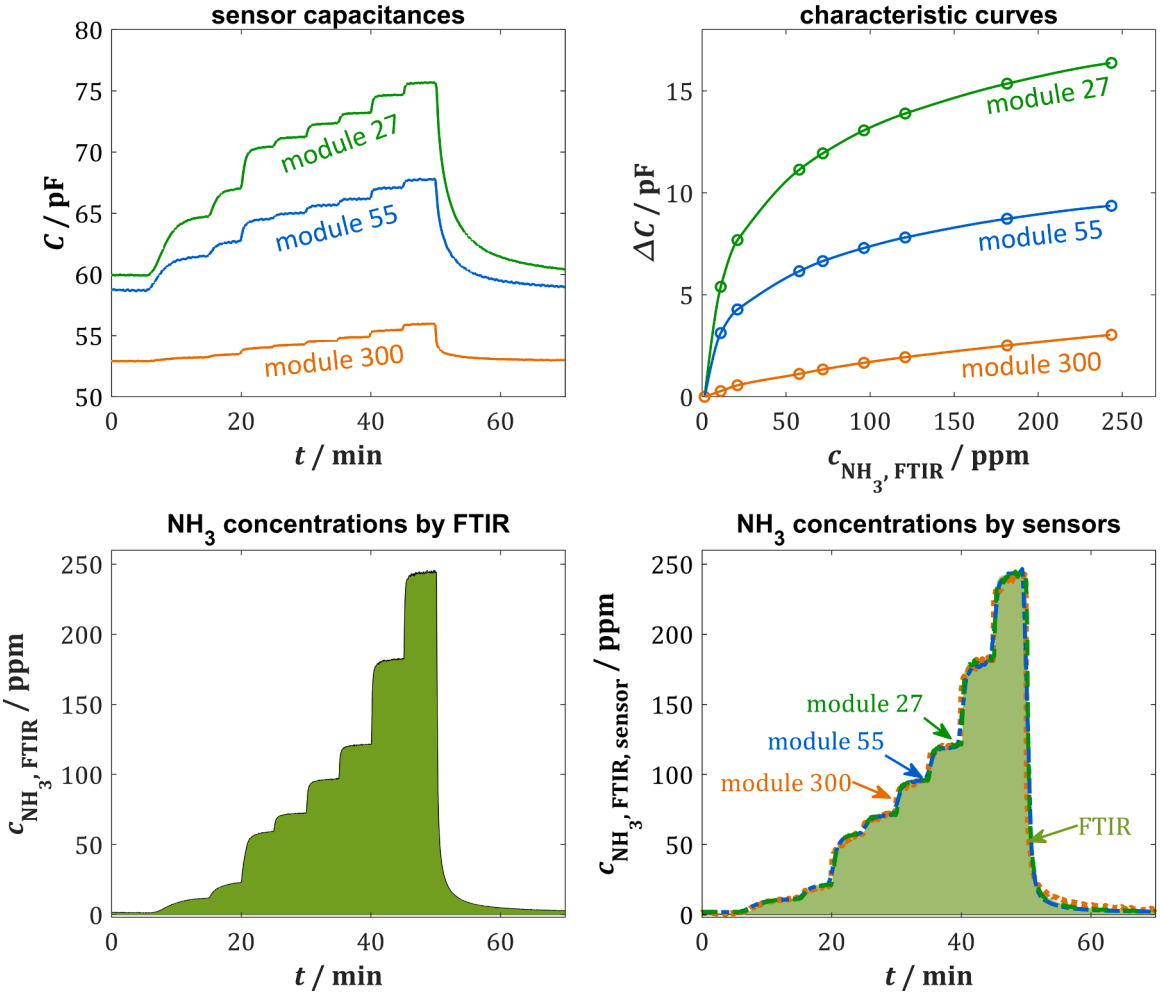

Fig. 3. a) Time course of the capacitance values of the different zeolite modules (27, 55, 300) and b) of the dosed NH_3 measured by the FTIR spectrometer downstream of the measurement chamber. c) Sensor responses depending on the ammonia concentration determined at steady state values from a) and b). d) Comparison of the NH_3 concentration measured by the sensors (calculated using the characteristic curves from c)) and the FTIR spectrometer over time, sensor temperature 400 °C, base gas composition: 10 vol% O_2, 3 vol% CO_2, 5 vol% H_2O in N_2. Measured at 700 kHz.

differences in ammonia sensitivity were observed between the zeolite modules. In particular, at low ammonia concentrations (less than 50 ppm), the change in capacitance was significantly higher for the sensor with a module of 27 than for those with modules of 55 or 300. As a consequence of the enhanced number of active centers resulting from the reduced zeolite module, there is a higher ability to adsorb ammonia [83]. Consequently, an increase in the sensor signal was detected.

The observed delay in the return of the capacitance to the base value at the end of ammonia dosing (at 52 minutes) can be attributed to damping effects of the gas dosing setup. Due to ammonia absorption and slow desorption on the walls of the piping and the sensor test bench, minor yet non-negligible concentrations remain present in the measuring chamber even several minutes after the end of dosing. This results in a higher signal response for the zeolites with a low module (27, 55), although this is not related to a slow response time of the sensor.

Fig. 3d illustrates a comparison of the ammonia concentrations over time, measured by the sensors and the FTIR spectrometer. For this purpose, the concentration actually measured by the respective sensor at each point in time of the measurement was calculated from the calibration curve as shown in Fig. 3c. This demonstrates that the curves between sensor response and FTIR data are nearly identical. The sensors thus exhibit a sufficient response time to enable the detection of rapid ammonia concentration fluctuations. The apparently slower return to the base capacitance value can therefore be attributed to a higher sensitivity of sensors with a low zeolite module at low NH_3 concentrations. In order to ensure an efficient control of AdBlue dosing, it is of critical importance to be able to detect even small ammonia concentrations (< 30 ppm) in the flue gas of combustion plants. At this stage of the investigation, the sensors with a zeolite module of 27 exhibited the most promising response, as the elevated number of active centers led to a significantly enhanced adsorption of ammonia. As a consequence, the electrical output signal for the particular sensor variant was higher. Nevertheless, further investigations are required to evaluate the influence of other gases and potential cross-sensitivities for the respective zeolite module.

3.2. Studies on cross-sensitivities

In addition to the sensitivity towards ammonia, the influence of other gas components also plays a significant role for the application in the flue gas of a biomass combustion system. During combustion, a wide range of gases are formed. Those components that are more likely to occur in real exhaust gases are investigated further. This included a variation of the previously used base gas components, which were CO_2, O_2, and H_2O. Furthermore, NO_x (consisting of NO and NO_2), CO, C_3H_8, and H_2 were admixed to the base gas.

In order to evaluate the cross-sensitivities, a sensor with a zeolite module of 27 was selected for demonstration purposes. Before the experiment, the sensor was calibrated at base gas (10 vol% O_2, 3 vol% CO_2, 5 vol% H_2O) as previously shown in Fig. 3c. The values shown in Fig. 4a again correspond to the actual ammonia concentrations measured by the sensor. Fig. 4b presents the actual gas concentrations determined by FTIR, with the exception of H_2, which was calculated from the mass flow data of the test bench.

The series of measurements was initiated with a variation of the NO, NO_2, and NH_3 concentration at base gas atmosphere. This sequence was then repeated twice, first with a change in the CO_2 (3–5 vol%) and O_2 (10–5 vol%) content, then with an increase in the water concentration

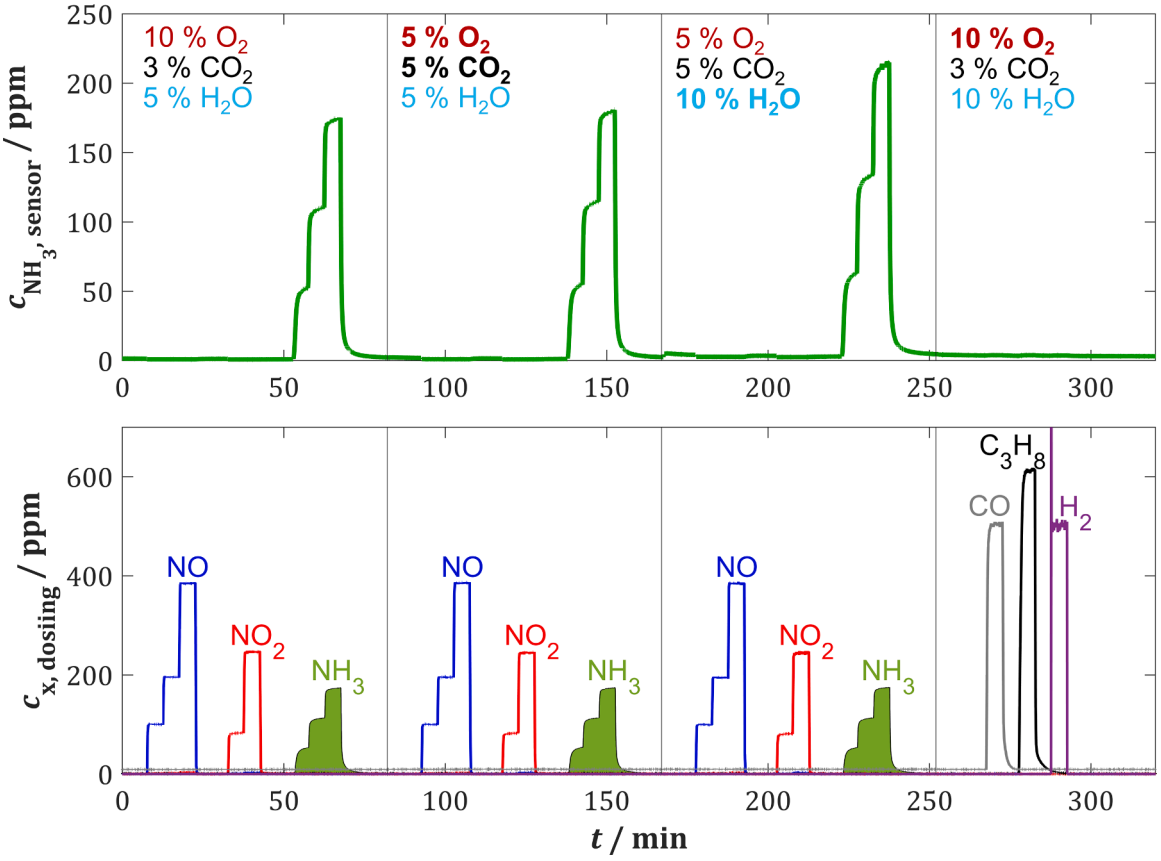

Fig. 4. Time course of a series of tests to investigate the cross-sensitivities under variation of the base gas components and dosing of other components relevant for biomass combustion. a) sensor data during variation of the base gas components (O_2, CO_2, H_2O) with NO_x and NH_3 dosing and subsequent exposure to CO, C_3H_8 and H_2 (calibration at base gas with 10 vol% O_2, 3 vol% CO_2, 5 vol% H_2O in N_2). b) dosed gas concentrations of the special gases (NH_3, NO_x, CO, C_3H8, H_2) measured by downstream FTIR spectrometer. Sensor temperature 400 °C, zeolite module 27.

(5–10 vol%). Subsequently, the sensors were briefly exposed to CO, C_3H_8, and H_2.

The results showed that the sensor responds with high selectivity to ammonia. A notable change in the sensor signal was observed specifically during dosing of NH_3. Furthermore, no notable influence was detected when NO_x, CO, C_3H_8, and H_2 were admixed.

In contrast, an apparent increase in the ammonia concentration occurred when the water content was increased from 5 to 10 vol%. This discrepancy between the measured and the actual ammonia concentrations may be attributed to the influence of water on the zeolite, since water is also capable of adsorbing onto the zeolite, following a mechanism similar to ammonia [84]. In order to investigate this effect in more detail, a series of measurements were carried out in which the NH_3 concentration was varied for different H_2O concentrations. Fig. 5a illustrates the typical response curves of a sensor with a module of 27 at water contents of 2, 5, and 10 vol%. An increase in the water content results in a slight shift of the characteristic curve to higher capacitance values of approximately 0.3 pF per percentage of water vapor for the sensor with a module of 27. This results in an increase in the measured ammonia concentration by the sensor in Fig. 4, as an increase in the water content is incorrectly interpreted as an increase in the ammonia concentration. While the influence of water is therefore significantly lower than that of ammonia, it cannot completely be neglected for the application. Fluctuations in water content of ± 2.5 vol% are to be expected in real biomass firing applications [85].

The results of this series of measurements indicate that further investigation of other gas components in combination with simultaneous dosing of ammonia should contribute to the sensor development for real-world applications. Of the gas components further investigated here (CO_2, O_2, NO_x, CO, C_3H_8 and H_2), however, only the combination of NO_x with NH_3 proved to be critical (see equations (1) and (2)). A corresponding series of measurements, similar to the procedure for analyzing the influence of water, can be seen in Fig. 5b.

The presence of NO resulted in a slight reduction of the sensor response. An additional increase in the NO concentration from 100 ppm to 200 ppm further reduced the response. This effect may be attributed to the occurrence of SCR reactions at the zeolite film according to equation (1). These reactions result in the conversion of ammonia molecules with nitrogen oxides into nitrogen and oxygen [60,86,87]. Consequently, the quantity of ammonia adsorbed on the zeolite layer decreased. Thus, the concentration indicated by the sensor was found to be lower than the actual concentration of ammonia present in the gas. This effect becomes even more pronounced when part of the NO concentration is replaced by NO_2. Now, the total concentration of 200 ppm NO_x was maintained, but 10 vol% (≙ 20 ppm) NO_2 were admixed, which is a typical value for the NO_2/NO_x-ratio in a real flue gas. As a consequence of the fast SCR reaction (see equation (2)), an increased conversion of NO_x and NH_3 at the zeolite was observed, which in turn led to a further decrease in the sensor signal.

In the following, the influence of the two gas components (NO_x and H_2O) was found to vary depending on the specific zeolite module selected for the gas sensitive film. The previously described series of measurements was thus repeated with the sensors made of zeolites with modules of 55 and 300. To classify the cross-sensitivities, the capacitance values of the sensors were calculated into the ammonia concentration using a calibration measurement determined at base gas. The change in the concentration values measured by the sensor in comparison to FTIR data when varying the water content (5–10 vol%) and when adding NO_x (200 ppm; 180 ppm NO and 20 ppm NO_2) can be found in Fig. 6.

As previously stated, with increasing water content, the ammonia concentration indicated by the sensor was in fact higher than the actual value. With increasing module, the resulting error also increased. The different influences observed with regard to the zeolite module are attributed to the varying types of bonding of the adsorbed gas species. While ammonia is typically bonded by van-der-Waals or covalent bonds, water is generally bonded to the zeolite via electrostatic attraction forces [81,88]. Also, the diffusion of gas species and the adsorption potential of individual molecules depend on many factors, including the zeolite module, pore size, temperature and the interaction of other molecules

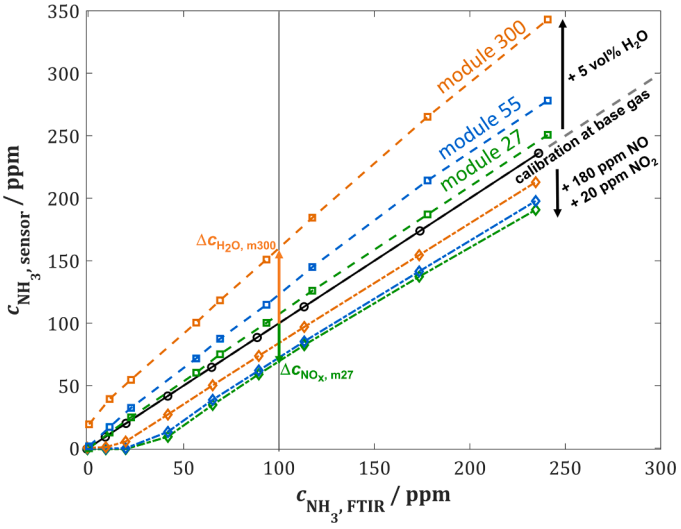

Fig. 6. Comparison of the ammonia concentration measured by the sensor and the FTIR when varying the water content from 5–10 vol% or when adding 200 ppm NO_x (180 ppm NO and 20 ppm NO_2). Calibration of the sensor with base gas with 10 vol% O_2, 3 vol% CO_2, 5 vol% H_2O in N_2, sensor temperature 400 °C.

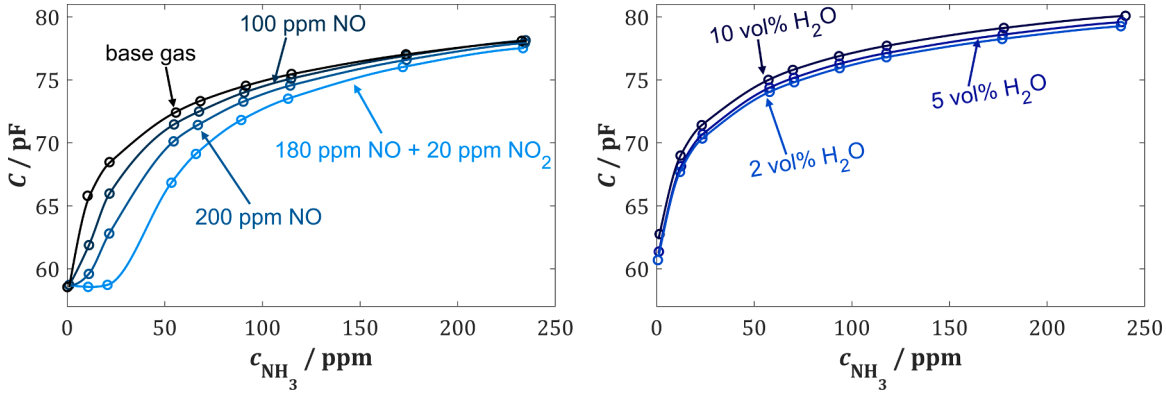

Fig. 5. Investigations of the influence of other gas components on the characteristic curve of the ammonia sensor. a) Variation of the water content. b) Variation of the NO_x concentration (NO, NO_2). Sensor temperature 400 °C, base gas composition: 10 vol% O_2, 3 vol% CO_2, 5 vol% H_2O in N_2, zeolite module 27.

with the zeolite structure [81,89]. This leads to a deviation that is dependent on the zeolite module when changes in the water content occur.

In general, the influence of water was found to be nearly linear for each zeolite module, while the sensitivity of ammonia decreases with increased ammonia concentration. This leads to an increased error for higher ammonia concentrations.

In contrast, the error caused by the presence of NO_x is observed to decrease with increasing zeolite module. While the zeolites with a module of 27 and 55 exhibited a comparable deviation in the characteristic curve, the error for the zeolite with a module of 300 was reduced to approximately half. The SCR reactions that occur require the presence of adsorbed ammonia on the zeolite [90,91]. As a consequence of the lower number of active centers, the probability of nitrogen oxide molecules being converted is reduced, given that significantly less ammonia adsorbs on the zeolite with a higher module [83]. This also results in a reduction of the converted ammonia, and in turn reduces the error when determining the ammonia concentration in NO and NO_2 containing ambiences.

Similar cross-sensitivities have been observed for other sensor principles when detecting ammonia in exhausts that contain water and/or nitrogen oxides.

In case of mixed potential sensors, an increase in the water content leads to a reduction in ammonia sensitivity, depending on the active layer used [92]. In real exhaust gas, however, this effect can be compensated by the influence of the oxygen content, at least to some extent. An increase in the oxygen concentration also leads to a reduction in ammonia sensitivity. The opposite trend of the water and oxygen content in the combustion exhaust gas in turn leads to a reduction in the error in the determination of the NH_3 concentration. [38,93]. As these two effects do not fully counterbalance each other, it is typically recommended to correct the signal by means of an additional signal or sensor, e.g., by a lambda probe [92].

The NO_x cross-sensitivity has an observable effect on various sensor variants, too, as it can result from SCR reactions or, as in case of the resistive VWT or mixed potential ammonia sensor, from different sorption or conversion processes of NO_x. This means that, in contrast to the sensor principle investigated here, these cross-sensitivities can usually be detected even in the absence of NH_3[39,44,94,95]. Similarly, the behavior of other sensors studied in literature can be influenced by adjusting various factors [96,97]. Such factors include the materials selected for the electrodes or the gas-sensitive film. In the case of sensors with VWT functional layers, the weight proportion of V_2O_5 is found to have an impact on the sensitivity to NH_3 [42,98]. Furthermore, the sensitivity and selectivity of the sensor can be influenced by the operating mode, for instance by applying a voltage or current bias [38,39].

A similar relationship with regard to existing cross-sensitivities can be observed with the zirconium oxide-based potentiometric NO_x sensor, which is commonly used in the automotive sector for SCR systems. This sensor also exhibits a high degree of cross-sensitivity to NH_3, which further depends on the concentration of NO_x present in the exhaust gas. According to measurements in the literature, the average influence of NH_3 on the measurement signal corresponds to about 2/3 of the effect of NO_x [99]. As previously stated, it is only possible to distinguish between the individual gas species despite the sum signal from NO_x and NH_3 by using complex, application-dependent models [100,101].

The results shown here indicate that the selection of the zeolite has a significant impact on the cross-sensitivities of the sensor. While zeolites with a low module showed the lowest water influence, they also demonstrated the highest error due to SCR activity. Consequently, a compromise is necessary, as certain changes in these exhaust gas components are to be expected in real applications. As the causes of the cross-sensitivity previously mentioned are considered to be temperature-dependent, the influence of the sensor operating temperature on the deviations resulting from H_2O and NO_x was investigated in further detail in the following section.

3.3. Studies on the influence of temperature on the response to NH_3 and on the cross-sensitivities

The operation temperature of exhaust gas sensors (T_H) is a crucial parameter that must be considered when evaluating the performance of such sensors. The effect of sensor temperature on the above-mentioned cross-sensitivities will now be investigated. As a measure of the cross-sensitivity of the sensor, the error in the determination of the concentration of ammonia under a change in the composition of the gas was considered. In order to achieve this, the difference between the actual concentration measured by the sensor and its calibration characteristic curve at 100 ppm ammonia was calculated. This value thus represents the error of the sensor reading at an actual ammonia concentration of 100 ppm (see Fig. 6 at 100 ppm NH_3).

Table 1 presents an error analysis conducted at temperatures between 360 and 480 °C for a 5 vol% change in the water content (from 5 vol% to 10 vol%).

The results showed that the responses for sensors containing a zeolite with a module of 27 in the low temperature range ($T_H < 440$ °C) and a zeolite with a module of 55 in the high temperature range ($T_H > 440$ °C) are only minimally affected by changes in the water content. The highest cross-sensitivity was identified, in analogy to the series of measurements illustrated in Fig. 6, for sensors with a zeolite film of module 300. This makes the zeolite with a module of 300 less suitable for use in real-world applications. Furthermore, the significantly reduced ammonia sensitivity, which is evident in Fig. 3, is a challenge for the measurement.

A more detailed examination of the change in capacitance caused by 100 ppm NH_3 displayed in Fig. 7 revealed that the two other zeolite variants demonstrated the highest measurement effect especially at low temperatures ($T_H < 420$ °C). Across the entire temperature range from 360 °C to 500 °C, the sensors comprising a zeolite with module 27 showed an approximately 50 % higher response compared to sensors with a zeolite module of 55.

However, an inverse correlation was observed with regard to the NO_x cross-sensitivity, as previously indicated. The SCR activity was found to be significantly lower for the zeolite with a module of 300. This result was also confirmed by the temperature-dependent error analysis in Table 2.

One can generally conclude that the addition of 200 ppm NO_x (180 ppm NO and 20 ppm NO_2) results in the largest error in the temperature range of approximately 440 °C for the zeolites under investigation. However, the data in Fig. 6 also confirmed that the zeolite with a module of 300 showed the smallest deviations from the actual ammonia concentration over the entire temperature range.

Given the preceding results that indicate that the use of sensors with a high zeolite module should be avoided due to the low ammonia sensitivity and the high water influence, the zeolite with a module of 27 is the most promising variant for future use in the flue gas of biomass combustion. Despite the fact that the NO_x cross-sensitivity for this zeolite module of 27 does not demonstrate a significant temperature dependency, an operation temperature below 440 °C should be preferred. In this temperature range, an increased ammonia sensitivity with a simultaneous decrease in water cross-sensitivity could be observed.

The cross-sensitivities investigated here are also discussed in the

Table 1
Temperature-dependent error analysis with a dosage of 100 ppm ammonia and an increase of the water concentration of 5 vol% for sensors with a zeolite module of 27, 55 and 300, base gas composition: 10 vol% O_2, 3 vol% CO_2, 5 vol % H_2O in N_2.

T_H / °C	360	400	440	480
$\Delta c_{H2O,\ m27}$ / ppm	6.8	9.8	13.8	15.6
$\Delta c_{H2O,\ m55}$ / ppm	14.2	23.0	8.6	6.7
$\Delta c_{H2O,\ m300}$ / ppm	53.0	60.1	57.6	80.5

literature, particularly with regard to sensor applications in combustion exhaust gas. In a previous study on a zeolite-based resistive ammonia sensor for automotive applications, cross-sensitivities to H_2O and NO_x were found to be comparable, while the influences of CO_2, O_2, and CO on the sensor signal were also negligible. Due to the more variable conditions present in the exhaust gas of combustion engines, particularly with regard to NO_x concentrations during load changes in comparison to almost constantly operated biomass combustion systems, a zeolite with a module of 140 was then selected for these investigations. In order to achieve an optimal balance between ammonia sensitivity, cross-sensitivities, and signal stability, a compromise was reached with this zeolite module [52,102]. However, for flue gas applications, H-ZSM-5 zeolites with a module of 27 are preferred. For this, a conclusive comparison in Table 3 includes the sensitivity, the selectivity (in form of the water cross-sensitivity), the NH_3 conversion, as well as the limit of detection (LOD) of sensors with the investigated zeolite modules for the preferred operating temperature of 400°C.

As previously mentioned, the zeolite with the lowest module (27) offers the highest NH_3 sensitivity in combination with the lowest water cross-sensitivity among the investigated zeolites. The factor Q_{H2O} that quantifies the water cross-sensitivity listed in Table 3 was calculated using Eq. (4).

$$Q_{H_2O} = \frac{\left(C(0\ \mathrm{ppm}_{NH_3},\ 5\ \mathrm{vol\%}_{H_2O}) - C(0\ \mathrm{ppm}_{NH_3},\ 2\ \mathrm{vol\%}_{H_2O})\right) \bullet 100\ \mathrm{ppm}_{NH_3}}{\left(C(100\mathrm{ppm}_{NH_3},\ 2\ \mathrm{vol\%}_{H_2O}) - C(0\ \mathrm{ppm}_{NH_3},\ 2\ \mathrm{vol\%}_{H_2O})\right) \bullet 3\ \mathrm{vol\%}_{H_2O}} \quad (4)$$

Q_{H2O} indicates a relative ratio between the changes in capacitance when the water content is increased by 3 vol% and a dosage of 100 ppm NH_3, in each case with the comparison to the initial value at 0 ppm NH_3 and 2 vol% H_2O. The higher water cross sensitivity of zeolites with higher modules is reflected by an increase of Q_{H2O} by a factor of 3 between sensors with a module of 27 and 300. Due to the higher sensor response, it is also possible to resolve lower concentrations of NH_3 using the sensor variant with a module of 27. The limit of detection (LOD) is three times lower in this case. However, this comes along with a higher error owing to NH_3 conversion in the presence of NO_x (calculated based on an underestimated sensor concentration at 100 ppm NH_3 and NO).

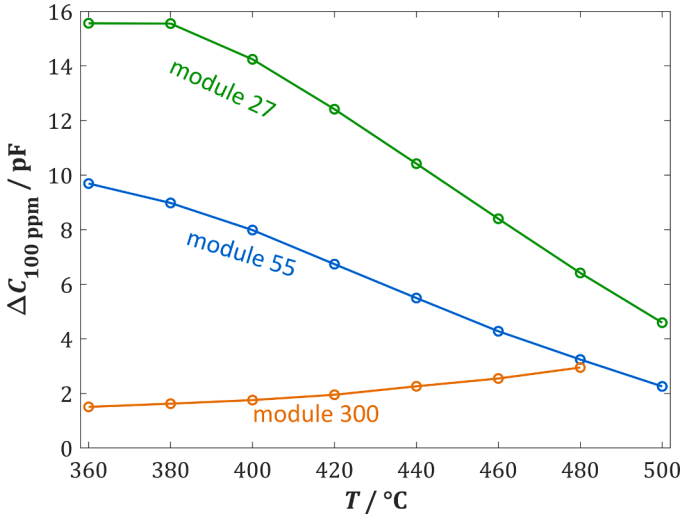

Fig. 7. Temperature-dependent change in capacity due to 100 ppm ammonia for sensors with different H-ZSM-5 zeolites with modules of 27, 55, and 300; base gas composition: 10 vol% O_2, 3 vol% CO_2, 5 vol% H_2O.

Table 2
Temperature-dependent error analysis due to the addition of 200 ppm NO_x (180 ppm NO and 20 ppm NO_2) with a dosage of 100 ppm ammonia for sensors with a zeolite module of 27, 55 and 300, base gas composition: 10 vol% O_2, 3 vol % CO_2, 5 vol% H_2O in N_2.

T_H / °C	360	400	440	480
$\Delta c_{NOx,\ m27}$ / ppm	−20.1	−28.4	−26.2	−23.5
$\Delta c_{NOx,\ m55}$ / ppm	−16.4	−26.8	−31.5	−26.4
$\Delta c_{NOx,\ m300}$ / ppm	−8.2	−15.2	−27.0	−13.5

The impact of the cross-sensitivities investigated within this study are affected by the application of the sensor under real conditions. In biomass combustion systems, such as biogas cogeneration plants, for example, the fuel is typically burned under constant conditions, meaning that fluctuations in the concentration of the relevant components during operation are minimal. In such systems, only a rudimentary knowledge of the occurring gas concentrations must therefore be known in order to provide a corresponding characteristic curve for the sensor.

In the case of boilers that cannot operate in a stationary condition with respect to the combustion process (e.g., pellet or wood chip firing systems), at least one secondary signal is required to correct the cross-sensitivity of the sensor. Plants in the power range of > 100 kW are often equipped with NO_x sensors in the flue gas pipe, allowing to correct the NO_x cross-sensitivity [32]. Additionally, with such a NO_x sensor the oxygen content in the flue gas can be determined, which is directly related to the water content [100,103], since an increased demand for oxygen reduces the residual oxygen content in the flue gas and increases the water content [104]. One approach to minimize the errors resulting from these two cross-sensitivities is to use the signal from a commercially available NO_x sensor. The integration of alternative data, such as fuel type, intake air control, and/or flue gas temperature, could also be evaluated. However, this approach requires a more precise understanding of the specific system in order to estimate H_2O and NO_x emissions. Typically, this demands a series of comprehensive measurements.

4. Conclusion and outlook

This work presented further investigations on the behavior of a zeolite-based ammonia sensor, which was operated as a capacitive sensor following detailed electrochemical impedance analysis. A particular focus of this study was on the influence of the zeolite functional film, and in particular the zeolite module, on the ammonia sensitivity and cross-sensitivities. In general, the sensors demonstrated

Table 3
Comparative overview of the three zeolite modules tested at a sensor temperature of 400 °C with regard to ammonia sensitivity, water cross-sensitivity (ratio of capacitance changes with a variation of 3 vol% H_2O and 100 ppm NH_3), average NH_3 conversion at 100 ppm NH_3 with 100 ppm NO and the limit of detection (LOD).

	Module 27	Module 55	Module 300
$\Delta C_{100\ ppm\ NH3}$ / pF	14.2	8.0	1.8
Q_{H_2O} / 10^{-4}	2.36	5.54	7.29
NH_3 conversion / %	9.13	8.67	1.30
LOD / ppm	0.85	2.71	2.86

cross-sensitivities to only a limited number of gas components. In addition to the known adsorption properties of zeolites towards water, the low SCR activity resulted in a reduction in the output signal when NO_x and NH_3 were simultaneously present in the gas. The extent of these cross-influences was found to vary according to the specific selected zeolite module. The cross-sensitivity of zeolites with a low module to changes in water content was found to be lower, but they showed higher deviations from the calibration value when dosing NO_x. In order to apply this in practice, a compromise must be reached in order to select a sensor variant with the lowest possible cross-sensitivity. Additionally, variations of the sensor operation temperature affected its cross-sensitivities.

In subsequent series of measurements, in addition to the cross-sensitivities investigated here, poisoning effects caused by HCl and SO_2 will also be investigated. They may lead to a permanent deactivation of the acid centers of the zeolite. Furthermore, long-term stability is also a challenge due to harsh flue gas conditions. Also, measurements are to be performed on exhaust gases from several biomass combustion plants that include the dosing of AdBlue. It is of significant importance to select an appropriate protective cap in order to ensure a rapid exchange of gases at the sensor surface. The impact of soot and dust particles, which may deposit on the sensor surface due to the relatively low operating temperature, must be considered, as these can potentially affect the sensor behavior.

CRediT authorship contribution statement

Hagen Gunter: Writing – review & editing, Methodology, Formal analysis, Conceptualization. **Wöhrl Thomas:** Writing – original draft, Visualization, Validation, Methodology, Investigation, Formal analysis, Conceptualization. **Moos Ralf:** Writing – review & editing, Supervision, Funding acquisition, Conceptualization.

Declaration of Competing Interest

The authors declare that they have no known competing financial interests or personal relationships that could have appeared to influence the work reported in this paper.

Acknowledgements

This work was supported by The Federal Ministry for Economic Affairs and Climate Action, Germany, project "Neue Sensorik für die Prozessoptimierung von SCR-Verfahren und Partikelabscheidung an Biomasseverbrennungsanlagen (BioFeuSe)", grant number 03EI5434B. The authors would like to thank J. Thiessen (Department of Chemical Engineering, Prof. Jess) for conducting the BET measurements. The authors would also like to thank E. Kita, J. Schneider (both Department of Functional Materials) and the Bavarian Polymer Institute (BPI) for the SEM sample preparation and characterization.

Author contributions

Ralf Moos and Gunter Hagen created the concept of the project and were responsible for funding acquisition. Methodology was developed by Gunter Hagen and Thomas Wöhrl in close discussion with Ralf Moos. Thomas Wöhrl constructed the setup, conducted the investigation process, and wrote the original draft. All the authors contributed to the interpretation of the data and to the review and editing of the final paper. Ralf Moos supervised the work.

Data availability

Data will be made available on request.

References

[1] I. Malico, N.R. Pereira, A.C. Gonçalves, A.M. Sousa, Current status and future perspectives for energy production from solid biomass in the European industry, Renew. Sustain. Energy Rev. 112 (2019) 960–977, https://doi.org/10.1016/j.rser.2019.06.022.

[2] M. Lauer, M. Dotzauer, M. Millinger, K. Oehmichen, M. Jordan, J. Kalcher, S. Majer, D. Thraen, The crucial role of bioenergy in a climate-neutral energy system in Germany, Chem. Eng. Technol. 46 (2023) 501–510, https://doi.org/10.1002/ceat.202100263.

[3] D. Taylor, K. Chong, M. Röder, Designing biomass policy: the political economy of renewable energy for net zero, WIREs Energy Environ. 13 (2024), https://doi.org/10.1002/wene.512.

[4] Z.J. Mather-Gratton, S. Larsen, N.S. Bentsen, Understanding the sustainability debate on forest biomass for energy in Europe: A discourse analysis, PloS One 16 (2021) e0246873, https://doi.org/10.1371/journal.pone.0246873.

[5] J. Full, M. Trauner, R. Miehe, A. Sauer, Carbon-Negative Hydrogen Production (HyBECCS) from Organic Waste Materials in Germany: How to Estimate Bioenergy and Greenhouse Gas Mitigation Potential, Energies 14 (2021) 7741, https://doi.org/10.3390/en14227741.

[6] M. Nelles, K. Deprie, H. Jalalipour, The role of biogenic wastes and residues in a climate-neutral society: carbon source, bioenergy and negative emissions, Waste Manag. Res. 41 (2023) 741–743, https://doi.org/10.1177/0734242X231161506.

[7] H. Beidaghy Dizaji, T. Zeng, V. Lenz, D. Enke, Valorization of residues from energy conversion of biomass for advanced and sustainable material applications, Sustainability 14 (2022) 4939, https://doi.org/10.3390/su14094939.

[8] A. Demirbas, Combustion characteristics of different biomass fuels, Prog. Energy Combust. Sci. 30 (2004) 219–230, https://doi.org/10.1016/j.pecs.2003.10.004.

[9] X. Ren, R. Sun, X. Meng, N. Vorobiev, M. Schiemann, Y.A. Levendis, Carbon, sulfur and nitrogen oxide emissions from combustion of pulverized raw and torrefied biomass, Fuel 188 (2017) 310–323, https://doi.org/10.1016/j.fuel.2016.10.017.

[10] S.V. Vassilev, D. Baxter, L.K. Andersen, C.G. Vassileva, An overview of the chemical composition of biomass, Fuel 89 (2010) 913–933, https://doi.org/10.1016/j.fuel.2009.10.022.

[11] M. Mladenovic, D. Dakic, S. Nemoda, M. Paprika, M. Komatina, B. Repic, A. Eric, The combustion of biomass - the impact of its types and combustion technologies on the emission of nitrogen oxide, Hem. Ind. 70 (2016) 287–298, https://doi.org/10.2298/HEMIND150409033M.

[12] M.A. Bagherian, K. Mehranzamir, A comprehensive review on renewable energy integration for combined heat and power production, Energy Convers. Manag. 224 (2020) 113454, https://doi.org/10.1016/j.enconman.2020.113454.

[13] M. König, M. Müller, I. Hartmann, Emission reduction process for the energetic use of biogenic residues, IOP Conf. Ser.: Earth Environ. Sci. 642 (2021) 1–10, https://doi.org/10.1088/1755-1315/642/1/012006.

[14] X. Zhang, B. Ojha, H. Bichlmaier, I. Hartmann, H. Kohler, Extensive gaseous emissions reduction of firewood-fueled low power fireplaces by a gas sensor based advanced combustion airflow control system and catalytic post-oxidation, Sensors 23 (2023) 4679, https://doi.org/10.3390/s23104679.

[15] P. Forzatti, Present status and perspectives in de-NO_x SCR catalysis, Appl. Catal. A: Gen. 222 (2001) 221–236, https://doi.org/10.1016/S0926-860X(01)00832-8.

[16] B. Guan, R. Zhan, H. Lin, Z. Huang, Review of state of the art technologies of selective catalytic reduction of NO_x from diesel engine exhaust, Appl. Therm. Eng. 66 (2014) 395–414, https://doi.org/10.1016/j.applthermaleng.2014.02.021.

[17] M. Zhu, J.-K. Lai, U. Tumuluri, M.E. Ford, Z. Wu, I.E. Wachs, Reaction pathways and kinetics for selective catalytic reduction (SCR) of acidic NO_x emissions from power plants with NH_3, ACS Catal. 7 (2017) 8358–8361, https://doi.org/10.1021/acscatal.7b03149.

[18] F. Martinovic, L. Castoldi, F.A. Deorsola, Aftertreatment technologies for diesel engines: an overview of the combined systems, Catalysts 11 (2021) 653, https://doi.org/10.3390/catal11060653.

[19] L.E. Gevers, L.R. Enakonda, A. Shahid, S. Ould-Chikh, C.I.Q. Silva, P.P. Paalanen, A. Aguilar-Tapia, J.-L. Hazemann, M.N. Hedhili, F. Wen, J. Ruiz-Martínez, Unraveling the structure and role of Mn and Ce for NO_x reduction in application-relevant catalysts, Nat. Commun. 13 (2022) 2960, https://doi.org/10.1038/s41467-022-30679-9.

[20] S. Zhao, J. Peng, R. Ge, S. Wu, K. Zeng, H. Huang, K. Yang, Z. Sun, Research progress on selective catalytic reduction (SCR) catalysts for NO_x removal from coal-fired flue gas, Fuel Process. Technol. 236 (2022) 107432, https://doi.org/10.1016/j.fuproc.2022.107432.

[21] S. Elkaee, A.D. Phule, J.H. Yang, Advancements in (SCR) technologies for NO_x reduction: a comprehensive review of reducing agents, Process Saf. Environ. Prot. 184 (2024) 854–880, https://doi.org/10.1016/j.psep.2024.02.046.

[22] G.G. Naik, H.M. Dharmadhikari, Methods for reducing NO_x and PM emissions in compression ignition engine: A review, Mater. Today.: Proc. 72 (2023) 1406–1412, https://doi.org/10.1016/j.matpr.2022.09.339.

[23] M. König, K. Eisinger, I. Hartmann, M. Müller, Combined removal of particulate matter and nitrogen oxides from the exhaust gas of small-scale biomass combustion, Biomass-.-. Convers. Biorefinery 9 (2019) 201–212, https://doi.org/10.1007/s13399-018-0303-0.

[24] A. Bologa, H.P. Rheinheimer, H.P. Paur, Influence of ESP collector configuration on reduction of particulate emissions from biomass combustion facility, J. Phys.: Conf. Ser. 1322 (2019) 12025, https://doi.org/10.1088/1742-6596/1322/1/012025.

[25] S. Prabhu S, K. Natesan, N. Shivappa Nayak, Effect of UWS spray angle and positioning of injector on ammonia concentration in Urea-SCR system, Mater.

Today.: Proc. 46 (2021) 8051–8055, https://doi.org/10.1016/j.matpr.2021.03.026.
[26] F. Millo, F. Sapio, B.P. Paradisi, A. Bianco, L. Postrioti, G. Buitoni, M. Tabarrini, C. Robino, Experimental and numerical analysis of an innovative mixer geometry for urea injection in SCR applications, Emiss. Control Sci. Technol. 8 (2022) 78–95, https://doi.org/10.1007/s40825-022-00207-8.
[27] A. Bekal, S.K. Karthick, Y. Rajeshirke, G. Balasubramaniam, M. Upadhyay, S. Bhandarkar, D. Kuvalekar, C. Mitra, Emission Measurement Considerations for Power Industry, in: M. Bose (Ed.), Proceedings of the 7th International Conference on Advances in Energy Research, Springer Singapore Pte. Limited, Singapore, 2021, pp. 201–210, https://doi.org/10.1007/978-981-15-5955-6_20.
[28] L. Hofmann, K. Rusch, S. Fischer, B. Lemire, Onboard Emissions Monitoring on a HD Truck with an SCR System Using NO_x Sensors, SAE Int. 113 (2004) 559–572, https://doi.org/10.4271/2004-01-1290.
[29] C.M. Schar, C.H. Onder, H.P. Geering, Control of an SCR catalytic converter system for a mobile heavy-duty application, IEEE Trans. Control Syst. Technol. 14 (2006) 641–653, https://doi.org/10.1109/TCST.2006.876634.
[30] B. Timmer, W. Olthuis, A. den van Berg, Ammonia sensors and their applications—a review, Sens. Actuators B: Chem. 107 (2005) 666–677, https://doi.org/10.1016/j.snb.2004.11.054.
[31] Z. Bielecki, T. Stacewicz, J. Smulko, J. Wojtas, Ammonia gas sensors: comparison of solid-state and optical methods, Appl. Sci. 10 (2020) 5111, https://doi.org/10.3390/app10155111.
[32] N. Docquier, S. Candel, Combustion control and sensors: a review, Prog. Energy Combust. Sci. 28 (2002) 107–150, https://doi.org/10.1016/S0360-1285(01)00009-0.
[33] C. Malins, A. Doyle, B.D. MacCraith, F. Kvasnik, M. Landl, P. Simon, L. Kalvoda, R. Lukas, K. Pufler, I. Babusík, Personal ammonia sensor for industrial environments, J. Environ. Monit. JEM 1 (1999) 417–422, https://doi.org/10.1039/A904846D.
[34] S. Aarya, Y. Kumar, R.K. Chahota, Recent advances in materials, parameters, performance and technology in ammonia sensors: a review, J. Inorg. Organomet. Polym. Mater. 30 (2020) 269–290, https://doi.org/10.1007/s10904-019-01208-x.
[35] S. Hong, M. Wu, Y. Hong, Y. Jeong, G. Jung, W. Shin, J. Park, D. Kim, D. Jang, J.-H. Lee, FET-type gas sensors: a review, Sens. Actuators B: Chem. 330 (2021) 129240, https://doi.org/10.1016/j.snb.2020.129240.
[36] A. Lloyd Spetz, J. Huotari, C. Bur, R. Bjorklund, J. Lappalainen, H. Jantunen, A. Schütze, M. Andersson, Chemical sensor systems for emission control from combustions, Sens. Actuators B: Chem. 187 (2013) 184–190, https://doi.org/10.1016/j.snb.2012.10.078.
[37] N. Miura, T. Sato, S.A. Anggraini, H. Ikeda, S. Zhuiykov, A review of mixed-potential type zirconia-based gas sensors, Ionics 20 (2014) 901–925, https://doi.org/10.1007/s11581-014-1140-1.
[38] K.P. Ramaiyan, J.A. Pihl, C.R. Kreller, V.Y. Prikhodko, S. Curran, J.E. Parks, R. Mukundan, E.L. Brosha, Response characteristics of a stable mixed potential ammonia sensor in simulated diesel exhaust, J. Electrochem. Soc. 164 (2017) B448–B455, https://doi.org/10.1149/2.1271709jes.
[39] P.K. Sekhar, E.L. Brosha, R. Mukundan, W. Li, M.A. Nelson, P. Palanisamy, F. H. Garzon, Application of commercial automotive sensor manufacturing methods for NO_x/NH_3 mixed potential sensors for on-board emissions control, Sens. Actuators B: Chem. 144 (2010) 112–119, https://doi.org/10.1016/j.snb.2009.10.045.
[40] D. Schönauer, K. Wiesner, M. Fleischer, R. Moos, Selective mixed potential ammonia exhaust gas sensor, Sens. Actuators B: Chem. 140 (2009) 585–590, https://doi.org/10.1016/j.snb.2009.04.064.
[41] N. Donker, D. Schönauer-Kamin, R. Moos, Mixed-potential ammonia sensor based on a dense yttria-stabilized zirconia film manufactured at room temperature by powder aerosol deposition, Sensors 24 (2024), https://doi.org/10.3390/s24030811.
[42] C. Wang, X. Li, F. Xia, H. Zhang, J. Xiao, Effect of V_2O_5-content on electrode catalytic layer morphology and mixed potential ammonia sensor performance, Sens. Actuators B: Chem. 223 (2016) 658–663, https://doi.org/10.1016/j.snb.2015.09.145.
[43] D. Rauch, G. Albrecht, D. Kubinski, R. Moos, A microwave-based method to monitor the ammonia loading of a vanadia-based SCR catalyst, Appl. Catal. B: Environ. 165 (2015) 36–42, https://doi.org/10.1016/j.apcatb.2014.09.059.
[44] D. Schönauer, I. Sichert, R. Moos, Vanadia doped tungsten–titania SCR catalysts as functional materials for exhaust gas sensor applications, Sens. Actuators B: Chem. 155 (2011) 199–205, https://doi.org/10.1016/j.snb.2010.11.046.
[45] R. Jonsson, P.H. Ho, A. Wang, M. Skoglundh, L. Olsson, The Impact of Lanthanum and Zeolite Structure on Hydrocarbon Storage, Catalysts 11 (2021) 635, https://doi.org/10.3390/catal11050635.
[46] A.A. Ahmed, Z.H. Yamani, Synthesis and characterization of SnO_2-modified ZSM-5 zeolite for hydrogen gas sensing, Mater. Chem. Phys. 259 (2021) 124181, https://doi.org/10.1016/j.matchemphys.2020.124181.
[47] S.N. Talapaneni, J. Grand, S. Thomas, H.A. Ahmad, S. Mintova, Nanosized Sn-MFI zeolite for selective detection of exhaust gases, Mater. Des. 99 (2016) 574–580, https://doi.org/10.1016/j.matdes.2016.03.035.
[48] T. Simons, U. Simon, Zeolites as nanoporous, gas-sensitive materials for in situ monitoring of $DeNO_x$-SCR, Beilstein J. Nanotechnol. 3 (2012) 667–673, https://doi.org/10.3762/bjnano.3.76.
[49] T. Simons, U. Simon, Zeolite H-ZSM-5: a microporous proton conductor for the in situ monitoring of $DeNO_x$-SCR, MRS Proc. 1330 (2011), https://doi.org/10.1557/opl.2011.1337.
[50] T. Wöhrl, J. Kita, R. Moos, G. Hagen, Capacitive, highly selective zeolite-based ammonia sensor for flue gas applications, Chemosensors 11 (2023) 413, https://doi.org/10.3390/chemosensors11070413.
[51] P. Chen, S. Schönebaum, T. Simons, D. Rauch, M. Dietrich, R. Moos, U. Simon, Correlating the integral sensing properties of zeolites with molecular processes by combining broadband impedance and DRIFT spectroscopy-a new approach for bridging the scales, Sensors 15 (2015) 28915–28941, https://doi.org/10.3390/s151128915.
[52] R. Moos, R. Müller, C. Plog, A. Knezevic, H. Leye, E. Irion, T. Braun, K.-J. Marquardt, K. Binder, Selective ammonia exhaust gas sensor for automotive applications, Sens. Actuators B: Chem. 83 (2002) 181–189, https://doi.org/10.1016/S0925-4005(01)01038-3.
[53] D. Santa Cruz-Navarro, M. Torres-Rodríguez, M. Gutiérrez-Arzaluz, V. Mugica-Álvarez, S.B. Pergher, Comparative study of Cu/ZSM-5 catalysts synthesized by two ion-exchange methods, Crystals 12 (2022) 545, https://doi.org/10.3390/cryst12040545.
[54] C. Baerlocher, L.B. McCusker, D.H. Olson. Atlas of Zeolite Framework Types, 6th ed., Elsevier, Amsterdam, London, New York, Oxford, Paris, Shannon, Tokyo, 2007.
[55] B. Bensafi, N. Chouat, F. Djafri, The universal zeolite ZSM-5: structure and synthesis strategies. a review, Coord. Chem. Rev. 496 (2023) 215397, https://doi.org/10.1016/j.ccr.2023.215397.
[56] M. Pérez-Page, J. Makel, K. Guan, S. Zhang, J. Tringe, R.H. Castro, P. Stroeve, Gas adsorption properties of ZSM-5 zeolites heated to extreme temperatures, Ceram. Int. 42 (2016) 15423–15431, https://doi.org/10.1016/j.ceramint.2016.06.193.
[57] Y. Zheng, X. Li, P.K. Dutta, Exploitation of unique properties of zeolites in the development of gas sensors, Sensors 12 (2012) 5170–5194, https://doi.org/10.3390/s120405170.
[58] X. Xu, J. Wang, Y. Long, Zeolite-based materials for gas sensors, Sensors 6 (2006) 1751–1764, https://doi.org/10.3390/s6121751.
[59] T. Jiang, F. Göltl, R.E. Bulo, P. Sautet, Effect of temperature on the adsorption of short alkanes in the zeolite SSZ-13—adapting adsorption isotherms to microporous materials, ACS Catal. 4 (2014) 2351–2358, https://doi.org/10.1021/cs500189v.
[60] J.R. Di Iorio, S.A. Bates, A.A. Verma, W.N. Delgass, F.H. Ribeiro, J.T. Miller, R. Gounder, The dynamic nature of brønsted acid sites in Cu–zeolites during NO_x selective catalytic reduction: quantification by gas-phase ammonia titration, Top. Catal. 58 (2015) 424–434, https://doi.org/10.1007/s11244-015-0387-8.
[61] L. Rodríguez-González, F. Hermes, M. Bertmer, E. Rodríguez-Castellón, A. Jiménez-López, U. Simon, The acid properties of H-ZSM-5 as studied by NH_3-TPD and ^{27}Al-MAS NMR spectroscopy, Appl. Catal. A: Gen. 328 (2007) 174–182, https://doi.org/10.1016/j.apcata.2007.06.003.
[62] A.S. Al-Dughaither, H. de Lasa, HZSM-5 zeolites with different SiO_2/Al_2O_3 ratios. Characterization and NH_3 desorption kinetics, Ind. Eng. Chem. Res. 53 (2014) 15303–15316, https://doi.org/10.1021/ie4039532.
[63] L. Rodríguez-González, U. Simon, NH_3 -TPD measurements using a zeolite-based sensor, Meas. Sci. Technol. 21 (2010) 1–7, https://doi.org/10.1088/0957-0233/21/2/027003.
[64] L. Rodríguez-González, E. Rodríguez-Castellon, A. Jimenez-Lopez, U. Simon, Correlation of TPD and impedance measurements on the desorption of NH_3 from zeolite H-ZSM-5, Solid State Ion. 179 (2008) 1968–1973, https://doi.org/10.1016/j.ssi.2008.06.007.
[65] M. Minissale, J.-B. Faure, A. Dunand, T. Angot, G. de Temmerman, R. Bisson, Sticking probability of ammonia molecules on Tungsten and 316L stainless steel surfaces, J. Phys. Chem. C. 124 (2020) 17566–17577, https://doi.org/10.1021/acs.jpcc.0c03313.
[66] T. Wöhrl, J. Herrmann, J. Kita, R. Moos, G. Hagen, Methods to investigate the temperature distribution of heated ceramic gas sensors for high-temperature applications, J. Sens. Sens. Syst. 12 (2023) 205–214, https://doi.org/10.5194/jsss-12-205-2023.
[67] C.M.A. Brett, Electrochemical impedance spectroscopy in the characterisation and application of modified electrodes for electrochemical sensors and biosensors, Molecules 27 (2022), https://doi.org/10.3390/molecules27051497.
[68] Y. Barsukov, J.R. Macdonald, Electrochemical impedance spectroscopy, Charact. Mater. (2012) 1–17, https://doi.org/10.1002/0471266965.com124.
[69] M.E. Franke, M. Sierka, U. Simon, J. Sauer, Translational proton motion in zeolite H-ZSM-5. Energy barriers and jump rates from DFT calculations, Phys. Chem. Chem. Phys. 4 (2002) 5207–5216, https://doi.org/10.1039/b205426d.
[70] M.E. Franke, U. Simon, Solvate-supported proton transport in zeolites, Chemphyschem 5 (2004) 465–472, https://doi.org/10.1002/cphc.200301011.
[71] T.C. Hoff, R. Thilakaratne, D.W. Gardner, R.C. Brown, J.-P. Tessonnier, Thermal stability of aluminum-rich ZSM-5 zeolites and consequences on aromatization reactions, J. Phys. Chem. C. 120 (2016) 20103–20113, https://doi.org/10.1021/acs.jpcc.6b04671.
[72] P. Chen, V. Rizzotto, K. Xie, U. Simon, Tracking mobile active sites and intermediates in NH_3-SCR over zeolite catalysts by impedance-based in situ spectroscopy, React. Chem. Eng. 4 (2019) 986–994, https://doi.org/10.1039/C8RE00283E.
[73] U. Simon, D. Sanders, J. Jockel, C. Heppel, T. Brinz, Design strategies for multielectrode arrays applicable for high-throughput impedance spectroscopy on novel gas sensor materials, J. Comb. Chem. 4 (2002) 511–515, https://doi.org/10.1021/cc020025p.
[74] B. Legras, I. Polaert, L. Estel, M. Thomas, Mechanisms Responsible for Dielectric Properties of Various Faujasites and Linde Type A Zeolites in the Microwave Frequency Range, J. Phys. Chem. C. 115 (2011) 3090–3098, https://doi.org/10.1021/jp111423z.

[75] J.M. Kalogeras, A. Vassilikou-Dova, Molecular Mobility in Microporous Architectures: Conductivity and Dielectric Relaxation Phenomena in Natural and Synthetic Zeolites, Cryst. Res. Technol. 31 (1996) 693–726, https://doi.org/10.1002/crat.2170310602.
[76] U. Simon, U. Flesch, Cation-cation interaction in dehydrated zeolites X and Y monitored by modulus spectroscopy, J. Porous Mater. 6 (1999) 33–40, https://doi.org/10.1023/A:1009637102831.
[77] F. Li, H. Wu, C. Hua, Y. Zheng, Ammonia adsorption-induced change in permittivity of zeolite Y in millimeter-wave band, Sens. Actuators A: Phys. 303 (2020) 111852, https://doi.org/10.1016/j.sna.2020.111852.
[78] P. Vooka, B. George, A direct digital readout circuit for impedance sensors, IEEE Trans. Instrum. Meas. 64 (2015) 902–912, https://doi.org/10.1109/TIM.2014.2361552.
[79] S. Malik, L. Somappa, M. Ahmad, T. Islam, M.S. Baghini, An accurate digital converter for lossy capacitive sensors, Sens. Actuators A: Phys. 331 (2021) 112958, https://doi.org/10.1016/j.sna.2021.112958.
[80] J. Pérez Sanjurjo, E. Prefasi, C. Buffa, R. Gaggl, A capacitance-to-digital converter for mems sensors for smart applications, Sensors 17 (2017), https://doi.org/10.3390/s17061312.
[81] S.A. Pullano, F. Falcone, D.C. Critello, M.G. Bianco, M. Menniti, A.S. Fiorillo, An affordable fabrication of a zeolite-based capacitor for gas sensing, Sensors 20 (2020), https://doi.org/10.3390/s20072143.
[82] D.T. Hayhurst, Gas adsorption by some natural zeolites, Chem. Eng. Commun. 4 (1980) 729–735, https://doi.org/10.1080/00986448008935944.
[83] M. Dietrich, D. Rauch, U. Simon, A. Porch, R. Moos, Ammonia storage studies on H-ZSM-5 zeolites by microwave cavity perturbation: correlation of dielectric properties with ammonia storage, J. Sens. Sens. Syst. 4 (2015) 263–269, https://doi.org/10.5194/jsss-4-263-2015.
[84] B. Hunger, M. Heuchel, S. Matysik, K. Beck, W.D. Einicke, Adsorption of water on ZSM-5 zeolites, Thermochim. Acta 269-270 (1995) 599–611, https://doi.org/10.1016/0040-6031(95)02541-3.
[85] R.S. Parmar, M. Welling, M.O. Andreae, G. Helas, Water vapor release from biomass combustion, Atmos. Chem. Phys. 8 (2008) 6147–6153, https://doi.org/10.5194/acp-8-6147-2008.
[86] A.L. Kustov, K. Egeblad, M. Kustova, T.W. Hansen, C.H. Christensen, Mesoporous Fe-containing ZSM-5 zeolite single crystal catalysts for selective catalytic reduction of nitric oxide by ammonia, Top. Catal. 45 (2007) 159–163, https://doi.org/10.1007/s11244-007-0258-z.
[87] A.-Z. Ma, W. Grünert, Selective catalytic reduction of NO by ammonia over Fe-ZSM-5 catalysts, Chem. Commun. (1999) 71–72, https://doi.org/10.1039/A807490I.
[88] J. Vermesse, D. Vidal, P. Malbrunot, Gas adsorption on zeolites at high pressure, Langmuir 12 (1996) 4190–4196, https://doi.org/10.1021/la950283m.
[89] A.J. Porter, S.L. McHugh, T. Omojola, I.P. Silverwood, A.J. O'Malley, The effect of Si/Al ratio on local and nanoscale water diffusion in H-ZSM-5: a quasielastic neutron scattering and molecular dynamics simulation study, Microporous Mesoporous Mater. 348 (2023) 112391, https://doi.org/10.1016/j.micromeso.2022.112391.
[90] D. Rauch, D. Kubinski, G. Cavataio, D. Upadhyay, R. Moos, Ammonia loading detection of zeolite SCR catalysts using a radio frequency based method, SAE Int. J. Engines 8 (2015) 1126–1135, https://doi.org/10.4271/2015-01-0986.
[91] T. Simons, P. Chen, D. Rauch, R. Moos, U. Simon, Sensing catalytic conversion: simultaneous DRIFT and impedance spectroscopy for in situ monitoring of NH_3–SCR on zeolites, Sens. Actuators B: Chem. 224 (2016) 492–499, https://doi.org/10.1016/j.snb.2015.10.069.
[92] Y. Zhang, Y. Liu, L. Wang, H. Zhou, W. Meng, Y. Li, Z. He, L. Dai, A mixed-potential type NH_3 sensors based on spinel Zn_2SnO_4 sensing electrode, Sens. Actuators B: Chem. 367 (2022) 132154, https://doi.org/10.1016/j.snb.2022.132154.
[93] Y. Wang, S. Yao, M. Shost, J.-H. Yoo, D. Cabush, D. Racine, R. Cloudt, F. Willems, AmmoniA Sensor for Closed-loop SCR control, SAE Int. J. Passeng. Cars - Electron. Electr. Syst. 1 (2009) 323–333, https://doi.org/10.4271/2008-01-0919.
[94] D. Schönauer, T. Nieder, K. Wiesner, M. Fleischer, R. Moos, Investigation of the electrode effects in mixed potential type ammonia exhaust gas sensors, Solid State Ion. 192 (2011) 38–41, https://doi.org/10.1016/j.ssi.2010.03.028.
[95] Y. Zhang, B. Xiao, L. Yang, A. Jiao, K. Li, C. Wu, R. Zhan, Z. Huang, H. Lin, Sensitivity and selectivity enhancement of the YSZ-based mixed-potential ammonia sensors with flame-spray-made double-sensing electrodes, Sens. Actuators B: Chem. 344 (2021) 130165, https://doi.org/10.1016/j.snb.2021.130165.
[96] M.S. Islam, A. Bhardwaj, L. Mathur, I.-H. Kim, J.-Y. Park, S.-J. Song, Effects of electrolyte variation on ammonia sensing temperature for $BiVO_4$ sensing electrode in mixed potential gas sensor, Sens. Actuators B: Chem. 371 (2022) 132504, https://doi.org/10.1016/j.snb.2022.132504.
[97] I. Lee, B. Jung, J. Park, C. Lee, J. Hwang, C.O. Park, Mixed potential NH_3 sensor with $LaCoO_3$ reference electrode, Sens. Actuators B: Chem. 176 (2013) 966–970, https://doi.org/10.1016/j.snb.2012.09.009.
[98] D. Schönauer-Kamin, M. Fleischer, R. Moos, Influence of the V_2O_5 content of the catalyst layer of a non-Nernstian NH_3 sensor, Solid State Ion. 262 (2014) 270–273, https://doi.org/10.1016/j.ssi.2013.08.035.
[99] A. Frobert, S. Raux, Y. Creff, E. Jeudy, About Cross-Sensitivities of NO_x Sensors in SCR Operation, SAE Technical Paper (2013), doi: 10.4271/2013-01-1512.
[100] B. Pla, P. Piqueras, P. Bares, A. Aronis, NO_x sensor cross sensitivity model and simultaneous prediction of NO_x and NH_3 slip from automotive catalytic converters under real driving conditions, Int. J. Engine Res. 22 (2021) 3209–3218, https://doi.org/10.1177/1468087420966406.
[101] G. Hommen, F. Kupper, X. Seykens, Robust, model-based urea dosing control for SCR aftertreatment systems using a cross-sensitive tailpipe NO_x sensor, SAE Tech. Pap. 2017 (2017) 01–0938, https://doi.org/10.4271/2017-01-0938.
[102] R. Moos, A brief overview on automotive exhaust gas sensors based on electroceramics, Int. J. Appl. Ceram. Technol. 2 (2005) 401–413, https://doi.org/10.1111/j.1744-7402.2005.02041.x.
[103] J. Riegel, H. Neumann, H.-M. Wiedenmann, Exhaust gas sensors for automotive emission control, Solid State Ion. 152-153 (2002) 783–800, https://doi.org/10.1016/S0167-2738(02)00329-6.
[104] J. Villeneuve, J.H. Palacios, P. Savoie, S. Godbout, A critical review of emission standards and regulations regarding biomass combustion in small scale units (<3 MW), Bioresour. Technol. 111 (2012) 1–11, https://doi.org/10.1016/j.biortech.2012.02.061.

Thomas Wöhrl obtained a Master's degree in Automotive and Mechatronics at the University of Bayreuth in 2021. He is currently employed as a research assistant at the Chair of Functional Materials at the University of Bayreuth. There he mainly deals with exhaust gas aftertreatment in combustion processes of biogenic residues and waste materials. A particular focus here is on the optimization of selective catalytic reduction (SCR) of nitrogen oxides (NO_x) and the development of sensors for the selective detection of ammonia (NH_3).

Ralf Moos received the Diploma degree in electrical engineering in 1989 and the Ph.D. degree from the University of Karlsruhe, Karlsruhe, Germany, where he conducted research on defect chemistry of titanates. He joined Daimler in 1995 and worked in the serial development of exhaust gas aftertreatment systems. In 1997, he switched over to Daimler Research, Friedrichshafen, Germany. As a team leader in gas sensors, he headed several projects in the field of exhaust gas sensing. In 2001, he was appointed head of the Department of Functional Materials (Chair) of the University of Bayreuth. His main research interests are materials, systems, and concepts for gas sensing, batteries and electrochemical processes.

Gunter Hagen received the diploma degree in materials science in 2003 and the Ph.D. degree in 2009 from the University of Bayreuth, Germany. He is a permanent member and senior scientist in the department of Functional Materials, dealing with different kinds of gas sensors, novel sensor and catalyst materials, and exhaust gas after treatment systems.